The dipole potential correlates with lipid raft markers in the plasma membrane of living cells[S]

Tamás Kovács,* Gyula Batta,[†] Florina Zákány,* János Szöllősi,*,[§] and Peter Nagy[1,*]

Department of Biophysics and Cell Biology* and MTA-DE Cell Biology and Signaling Research Group,[§] Faculty of Medicine, and Department of Genetics and Applied Microbiology,[†] Faculty of Science and Technology, University of Debrecen, Debrecen, Hungary

Abstract The dipole potential generating an electric field much stronger than any other type of membrane potential influences a wide array of phenomena, ranging from passive permeation to voltage-dependent conformational changes of membrane proteins. It is generated by the ordered orientation of lipid carbonyl and membrane-attached water dipole moments. Theoretical considerations and indirect experimental evidence obtained in model membranes suggest that the dipole potential is larger in liquid-ordered domains believed to correspond to lipid rafts in cell membranes. Using three different dipole potential-sensitive fluorophores and four different labeling approaches of raft and nonraft domains, we showed that the dipole potential is indeed stronger in lipid rafts than in the rest of the membrane. The magnitude of this difference is similar to that observed between the dipole potential in control and sphingolipid-enriched cells characteristic of Gaucher's disease. The results established that the heterogeneity of the dipole potential in living cell membranes is correlated with lipid rafts and imply that alterations in the lipid composition of the cell membrane in human diseases can lead to substantial changes in the dipole potential.—Kovács, T., G. Batta, F. Zákány, J. Szöllősi, and P. Nagy. **The dipole potential correlates with lipid raft markers in the plasma membrane of living cells. *J. Lipid Res.* 2017.** 58: **1681–1691.**

Supplementary key words fluorescence and confocal imaging • fluorescence microscopy • Gaucher's disease • lipid rafts • membranes • membrane dipole potential

The eukaryotic cell membrane is a highly complex structure because of its lateral heterogeneity, the presence of membrane microdomains, and the "trinity" of membrane potentials, including transmembrane, surface, and dipole potentials (1, 2). The dipole potential is an intramembrane electrostatic potential that originates from the preferential alignment of interfacial water dipoles and dipolar segments of the lipid molecules with a negative contribution originating from phospholipid head group P^-–N^+ dipoles. Resulting from the arrangement of molecular dipoles, the interior part of the bilayer is characterized by a large positive dipole potential with a magnitude usually estimated in the range of several hundred millivolts, that is, a value that is much higher than that of transmembrane or surface potentials. As the dipole potential drops over a very short distance (2 and 3 nm, the approximate thickness of the monolayers in a bilayer) through the low dielectric hydrophobic interior of a membrane, it results in a large electrostatic dipole electric field (which is the spatial derivative of the potential) that a variety of experimental and computational techniques have estimated to be in the range of 10^8–10^9 V/m. This is significantly larger than either of the other two electrostatic fields associated with the transmembrane and surface potentials (estimated to be around $2.5 \cdot 10^7$, and 10^6 V/m, respectively) (1–5). Because of this large electric field, the dipole potential is considered to be essential for the conformation and the function of membrane proteins, and more generally for interactions between a lipid membrane and biological molecules embedded in a membrane, possibly influencing the distribution of proteins between different membrane regions and microdomains. Thus, the dipole potential was shown to influence the membrane permeability of large hydrophobic ions (6), to affect membrane binding of drugs (7), to modulate the conductance and association of ionophores (8), to play a role in the gating mechanism and conformational changes of voltage-gated ion channels (9), and to alter the activity of Na^+/K^+ ATPase (10) and P-glycoprotein (11). We have recently shown that alterations in the dipole potential change the ligand-binding affinity of epidermal growth factor receptor (ErbB1) and the ligand-induced clustering and activation of ErbB1 and ErbB2 and

This work was supported by research grants from the National Research, Development and Innovation Office, Hungary (K120302, GINOP-2.3.2-15-2016-00020, GINOP-2.3.2-15-2016-00044) and through the New National Excellence Program of the Ministry of Human Capacities.

Manuscript received 27 April 2017 and in revised form 6 June 2017.

Published, JLR Papers in Press, June 12, 2017
DOI https://doi.org/10.1194/jlr.M077339

Abbreviations: CBE, conduritol B epoxide; CTX, cholera toxin; GFP, green fluorescent protein; GPI, glycosylphosphatidylinositol.

[1] To whom correspondence should be addressed.
e-mail: nagyp@med.unideb.hu

[S] The online version of this article (available at http://www.jlr.org) contains a supplement.

that the extent of these effects depends on whether the proteins are localized in or outside of lipid rafts (12).

The dipole potential varies both longitudinally and laterally across the bilayer according to membrane composition and phospholipid packing density (1–5, 13). This phenomenon is the basis for artificially decreasing and increasing the dipole potential by phloretin and 6-ketocholestanol, respectively (14, 15). Besides the experimental manipulation, the dependence of the dipole potential on the lipid composition is expected to lead to different dipole potential values in different microdomains of the membrane. Indeed, cholesterol has been shown to increase the dipole potential because of its intrinsic dipole moment and its effects on the compaction and physical properties of the membrane (16). Apart from its effect on the dipole potential, cholesterol is known to induce the separation of liquid-ordered and -disordered domains in model membranes (17). Although liquid-ordered domains were shown to correspond to lipid rafts in cell membranes (18), this correlation remains highly speculative and contentious. The source of the confusion is the striking difference between the stability and size of liquid-ordered domains in model membranes and lipid rafts in cell membranes (19). Most researchers agree that lipid rafts are thermodynamically unstable, with sphingolipid and cholesterol-enriched microdomains in cell membranes exhibiting certain dynamic properties similar to those of liquid-ordered, stable domains in model membranes. However, lipid-mediated interactions are most likely not primarily responsible for the generation of lipid rafts, because the cytoskeleton, membrane proteins, their interactions with lipids, and membrane turnover all contribute to the properties and existence of rafts (19–22). Despite this controversy, a huge variety of biological functions, including transmembrane signaling and membrane trafficking, have been linked to lipid rafts in health and disease (23, 24).

Because the dipole potential is entirely located within the low dielectric, hydrophobic interior of the plasma membrane, it is difficult to measure directly. All of the methods described for the estimation of the dipole potential, including the measurement of the permeability of large hydrophobic ions (25), cryoelectron microscopy (26), molecular dynamics simulations (27, 28), atomic force microscopy (29), and vibrational Stark effect spectroscopy (30), are characterized by serious difficulties and disadvantages considering their applicability to living cells. Therefore, we opted for the fast-sensing voltage-sensitive fluorophores for measuring the dipole potential of living cells. The response of di-8-ANEPPS, a 4-p-aminostyryl-1-pyridinium derivative, to changes in the local electric field is based on electrochromism, and its emission measured at two different excitation wavelengths is sensitive to the dipole potential (12, 14, 15). The sensitivity of di-8-ANEPPS to changes in membrane fluidity (14) required the design of a new class of dipole potential-sensitive dyes. 3-Hydroxyflavone derivatives are characterized by two well-separated bands in their emission spectra belonging to normal (N*) and tautomer (T*) excited states of their flavone chromophore. Species T* appears as a result of an excited-state intramolecular proton transfer (ESIPT) reaction that is very sensitive to changes in the local electric field. The relative intensities of N* and T* fluorescence emission bands can be used to measure the dipole potential. Various 3-hydroxyflavone derivatives have been designed in which the chromophore is oriented in opposite directions with respect to the bilayer plane. Consistently, the N*:T* emission ratio of PPZ8 and of its related analog, F66, change in opposite directions upon modifying the dipole potential (31–33).

Alterations in the lipid composition of the membrane are associated with certain diseases (24). Gaucher's disease is a lysosomal storage disorder in which glucosylceramide accumulates because of a deficiency of glucocerebrosidase (34). Although symptoms are usually believed to be caused by the storage of glucosylceramide, weak or no correlation among the severity of symptoms, residual enzyme activity, and the amount of stored lipid casts doubt on the causative relationship (35). Gross alterations in lysosomal degradation of various substances due to "jamming" of the endosomal pathway and endoplasmic reticulum stress have also been invoked to explain the development of disease symptoms (36, 37). Elevated sphingolipid levels, observed in the plasma membrane in cellular models of Gaucher's disease (38, 39), are expected to alter the dipole potential as well.

Selective labeling of lipid rafts is based on the preferential concentration of certain membrane components in them. The incorporation of glycosylphosphatidylinositol (GPI)-anchored proteins into lipid rafts is driven by their lipid moiety. Various studies suggest that GPI-anchored proteins might rather be entrapped into "transient confinement zones" generated by the barrier effects of the cortical matrix, including the actin cytoskeleton and spectrin meshwork. The link between these compartments and lipid rafts remains unclear, but according to the operational definition of lipid rafts given above, cytoskeleton-mediated effects also contribute to the formation of raft-like microdomains (40, 41). Subunit B of cholera toxin (CTX-B) has also been widely used as a marker of lipid rafts because of its selective binding to GM1 ganglioside (42). Because of its multivalence, it can induce lipid reorganization into coexisting liquid-ordered and liquid-disordered fractions due to GM1 crosslinking (43, 44).

Although based on the differences in the lipid composition of raft-like microdomains and the bulk phase of the membrane, the assumption of a larger dipole potential in rafts seems logical, but this relationship has not been demonstrated directly in living cell membranes. Heterogeneity observed in the dipole potential has been assumed to be caused by lipid rafts, but explicit proof and quantitative analysis of this correlation has not been presented (1, 7, 45). On the other hand, the correspondence between electrostatic and topographic maps created by atomic-force microscopy performed with model membranes suggested that the dipole potential is larger is liquid-ordered domains (29).

On the basis of the correlation between the dipole potential reported by three different, ratiometric, dipole potential-sensitive dyes and the distribution of lipid rafts labeled by CTX-B, GPI-anchored green fluorescent protein (GFP), or an anticholesterol antibody, we show that the

dipole potential is significantly larger in lipid rafts than in the rest of the membrane. The fact that the magnitude of this difference is similar to the alteration in the dipole potential brought about by the increased sphingolipid concentration in Gaucher's disease points to a potential pathophysiological role for these findings.

MATERIALS AND METHODS

Cells, plasmids, and reagents

The human breast cancer cell line SKBR-3, the human epithelial carcinoma cell line A431, and the human acute monocytic leukemia-derived cell line THP-1 were obtained from the American Type Culture Collection (Manassas, VA) and grown according to their specifications. AlexaFluor647-tagged CTX-B was purchased from ThermoFisher (Waltham, MA). The GFP-GPI plasmid was a kind gift from Jennifer Lippincott-Schwartz (National Institutes of Health, Bethesda, MD), and the anticholesterol antibody was provided by János Matkó (Eötvös Loránd University, Budapest, Hungary). AlexaFluor647-transferrin was purchased from ThermoFisher. 6-Ketocholestanol (3β-hydroxy-5α-cholestan-6-1) and Pluronic F-127 were purchased from Sigma Aldrich (St. Louis, MO), and di-8-ANEPPS (4-(2-[6-(dioctylamino)-2-naphtalenyl] ethenyl)-1-(3-sulfopropyl)pyridinium inner salt) was acquired from ThermoFisher. F66 (N-[3-(40-dihexylamino-3-hydroxy-flavonyl-6-oxy)-propyl]N,N-dimethyl-N-(3-sulfopropyl)-ammonium, inner salt) and PPZ8 (3-[4-(4-[4V-(3-hydroxy-6-octyloxyflavonyl)phenyl] piperazino)-1-pyridiniumyl]-1-propanesulfonate) were kind gifts from Andrey Klymchenko (Université de Strasbourg, Strasbourg, France). The protein kinase C activator phorbol 12-myristate 13-acetate (PMA) and the β-glucosidase inhibitor conduritol B epoxide (CBE) were purchased from Sigma Aldrich.

Labeling of raft and nonraft domains

Lipid rafts were labeled with one of three different methods. *i*) GM1-enriched membrane rafts were labeled by incubating cells grown on 8-well chambered coverglass in the presence of 8 μg/ml AlexaFluor647-CTX-B for 20 min on ice to prevent internalization of CTX-B. *ii*) For labeling lipid rafts with GFP-GPI, SKBR-3 and A431 cells grown on 8-well chambered coverglass were transfected with 0.5 μg GFP-GPI plasmid/well using Lipofectamine2000 (ThermoFisher) at a lipid to DNA ratio of 2:1 (v/w). The transfection protocols were otherwise according to the manufacturer's specifications. *iii*) The cholesterol component of lipid rafts was visualized with AC8, a cholesterol-specific monoclonal antibody (46), followed by secondary labeling with the Fab fragment of Cy5-conjugated goat anti-mouse IgG (ThermoFisher) to minimize crosslinking. Alternatively, transferrin residing outside lipid rafts (47) was labeled with 25 μg/ml AlexaFluor647-conjugated transferrin (ThermoFisher) on ice. After labeling cells with one of the aforementioned indicators and a dipole potential-sensitive dye, images were taken with an LSM880 confocal laser-scanning microscope (Carl Zeiss AG, Jena, Germany). AlexaFluor647 and Cy5 were excited at 633 nm, and their emission was detected between 649 and 759 nm, whereas GFP was excited at 488 nm, and its emission was detected between 506 and 555 nm.

Altering the dipole potential

The dipole potential was increased by treating SKBR-3 and A431 cells with 6-ketocholestanol at a concentration of 100 μM for 10 min at room temperature in the presence of 0.05% (v/v) Pluronic F-127 (12, 14).

Measuring the dipole potential with di-8-ANEPPS

For measuring the dipole potential with di-8-ANEPPS, we grew SKBR-3 and A431 cells, as well as control and CBE-treated THP-1-derived macrophages, on 8-well chambered coverglass, then incubated them with 2 μM di-8-ANEPPS (with or without CTX-B) for 20 min on ice, and their fluorescence was measured with a ratiometric assay shown to be responsive to changes in the dipole potential (15). The dye was excited at 458 and 514 nm, and its emission was measured between 584 and 686 nm. Image acquisition was performed using an LSM880 confocal laser-scanning microscope. Image processing was carried out with the DipImage toolbox (Delft University of Technology, Delft, The Netherlands) under MATLAB (MathWorks, Natick, MA). The fluorescence intensity ratio (exc458/514) of the cell membrane pixels, calculated after background subtraction, is expected to show positive correlation with the dipole potential (15, 48).

Measuring the dipole potential with F66 and PPZ8

For measuring the dipole potential with F66 and PPZ8, we grew SKBR-3 and A431 cells, as well as control and CBE-treated differentiated THP-1 cells on 8-well chambered coverglass, then incubated them with 10 nM F66 or PPZ8 (with or without CTX-B) for 20 min on ice, and their fluorescence was measured with a ratiometric assay shown to be responsive to changes in the dipole potential (31, 49). The dye was excited at 405 nm, and its emission was measured in two different wavelength ranges, 463–527 and 543–589 nm. Image acquisition was performed using an LSM880 confocal laser-scanning microscope. Image processing was carried out with the DipImage toolbox under MATLAB. The fluorescence intensity ratio (em463–527:543–589) of the cell membrane pixels was calculated after background subtraction. The emission ratios of F66 and PPZ8 are expected to be negatively and positively correlated with the dipole potential, respectively (31, 49).

Determination of the correlation coefficient between the dipole potential and the lipid rafts

The dipole potential of SKBR-3 and A431 cells was measured with di-8-ANEPPS, and lipid rafts were labeled with CTX-B or GFP-GPI. Alternatively, F66 was used for measuring the dipole potential, with CTX-B for labeling lipid rafts. Images were acquired from the flat, bottom membrane of cells adjacent to the coverslip. During image processing the cell was circumscribed, providing a "cell mask." Another mask was defined by ignoring the brightest patches within the cell mask. The calculations were carried out only in these two regions. The Pearson correlation coefficient between the intensity ratio characterizing the dipole potential and the fluorescence intensity of lipid rafts was determined from pixelwise data of individual cells by using a custom-written algorithm under MATLAB. The confidence interval of the correlation coefficient assuming no correlation between the analyzed parameters was also determined for each image according to the method of Costes (50). The correlation coefficient between two lipid raft labels, GFP-GPI and CTX-B, was used as a positive control.

Determination of the dipole potential in raft versus nonraft membrane regions

The dipole potential was determined in the "raft" and "nonraft" regions of SKBR-3 and A431 cells. Images were acquired from the bottom of the cells. During image analysis, segmentation of images was carried out using a custom-written MATLAB algorithm. A threshold intensity was determined for lipid raft labels (CTX-B or GFP-GPI) using the maxentropy algorithm confirmed by visual inspection. Pixels were considered "raft" or "nonraft" pixels if their intensity was above or below the determined threshold, respectively. Average di-8-ANEPPS and F66 intensity ratios

JOURNAL OF LIPID RESEARCH ASBMB JLR

were separately determined from individual pixels in the "raft" and "nonraft" regions. Alternatively, the emission spectrum of F66 or PPZ8 was measured in the 468–621 nm range in 9 nm intervals at an excitation wavelength of 405 nm using the lambda-mode of LSM880. In these experiments the emission spectrum was evaluated inside and outside lipid rafts in a manner identical to what was described for the intensity ratio.

Determination of the dipole potential in control versus Gaucher-type THP-1-derived macrophages

THP-1 monocytes were differentiated into macrophages by PMA treatment (50 ng/ml for 5 days) to ensure their attachment to coverslips and so that they could be used as a model system for Gaucher disease by treating them with 500 μM CBE together with PMA (39). The average dipole potential was determined in control and Gaucher-type macrophages using di-8-ANEPPS, F66, or PPZ8 labeling, followed by acquiring images from the midplane of the cells. During processing, segmentation of images into membrane and nonmembrane pixels was carried out with the manually seeded watershed algorithm using a custom-written MATLAB program as described previously (51). The average fluorescence intensity ratio of the cell membrane pixels, characterizing the dipole potential, was calculated after background subtraction.

RESULTS

Emission ratiometric dyes respond to changes in the dipole potential

In the first part of our experiments, we tested whether two voltage-sensitive fluorophores, PPZ8 and F66, in which the fluorophore is oriented oppositely with respect to the membrane normal, are suitable for determining changes in the dipole potential in living cell membranes. After treating A431 and SKBR-3 cells with 6-ketocholestanol, known to increase the dipole potential, we recorded images from the flat membrane of the cells adjacent to the coverslip (supplemental Fig. S1). Fluorescence emission was measured in two wavelength ranges, corresponding to the N* and T* bands, and the ratio of the two intensities was determined on a pixel-by-pixel basis. Consistent with our expectations, 6-ketocholestanol significantly increased the N*:T* intensity ratio of PPZ8 while decreasing it in the case of F66 (**Fig. 1**). Both the shift in the pixelwise distribution of the emission ratio and changes in its mean confirm that PPZ8 and F66 can be used to determine changes in the dipole potential in living cells via an emission ratiometric method using confocal microscopy.

Correlation of the dipole potential with the distribution of markers for raft and nonraft domains

To test the hypothesis that the largely different lipid composition of rafts leads to a higher dipole potential than in the bulk phase of the membrane, we examined the correlation between the ratiometric response of three dyes with the intensities of lipid raft markers in the membranes of living A431 and SKBR-3 cells by determining the correlation coefficient between the intensity ratios of voltage-sensitive fluorophores and commonly used raft markers, AlexaFluor647-labeled CTX-B or GFP-GPI. The chromophore groups of PPZ8 and di-8-ANEPPS are oriented parallel to each other, whereas the fluorophore of F66 is aligned in the opposite direction. As a positive control, we determined the correlation coefficient between the two raft markers. Cells were transfected with GFP-GPI and labeled with CTX-B, and images were recorded of the flat, bottom membrane region adjacent to the coverslip. The Pearson correlation coefficient between the pixelwise intensities of the two raft markers was 0.55 ± 0.04 in A431 and 0.48 ± 0.03 in SKBR-3 cells (**Table 1**). The fact that these correlation coefficients are far outside the confidence intervals of the correlation coefficient, assuming no correlation, and the corresponding contour plots showing the distribution of individual pixel intensities (supplemental Fig. S2) confirm a strong positive correlation and allowed us to conclude that the method can be used to examine the correlation between two signals in living cells.

Then, we determined the relationship between the dipole potential and the intensity of raft markers. Cells were labeled by one of the three dipole potential-sensitive fluorophores, and the intensity ratios proportional to the dipole potential were determined on a pixel-by-pixel basis, and their correlation with the intensity of the raft marker (CTX-B, GFP-GPI, or anticholesterol mAb) was calculated. The excitation ratio of di-8-ANEPPS showed a positive correlation with each of the lipid raft markers (Table 1, supplemental Fig. S2). On the contrary, the F66 N*:T* emission ratio correlated negatively with the intensity of CTX-B (Table 1, supplemental Fig. S2). The smaller correlation coefficients obtained for the anticholesterol mAb may be due to the lower fluorescence intensity and consequently poorer image quality compared with the other raft markers. The statistical significance of these findings is supported by the fact that the calculated correlation coefficients are outside the confidence intervals determined for the absence of correlation. Their biological significance is underlined by the fact that the correlation coefficients between the dipole potential and the raft markers are similar to what was determined between the two lipid raft markers. The correlation of the intensity ratio of F66 with the GFP-GPI intensity or the intensity of the anticholesterol antibody was not examined because of the spectral overlap between the fluorophores. We also investigated the relationship between the dipole potential reported by PPZ8 and the lipid raft marker, CTX-B, and a negative correlation was observed (Table 1). Because the chromophore in F66 is oriented oppositely to that in di-8-ANEPPS and PPZ8 with respect to the membrane bilayer, the dipole potential correlates positively with the intensity ratio of di-8-ANEPPS and PPZ8 and negatively with the emission ratio of F66. It follows from this relationship that the results obtained with the two oppositely oriented dipole potential-sensitive fluorophores, di-8-ANEPPS and F66, imply that the magnitude of the dipole potential correlates with the presence of raft microdomains, whereas the results obtained with PPZ8 contradict this conclusion, which is resolved in the next section and in the discussion.

Although we had to record images from the flat membrane adjacent to the coverslip to observe the correlation between lipid rafts and the dipole potential, this approach

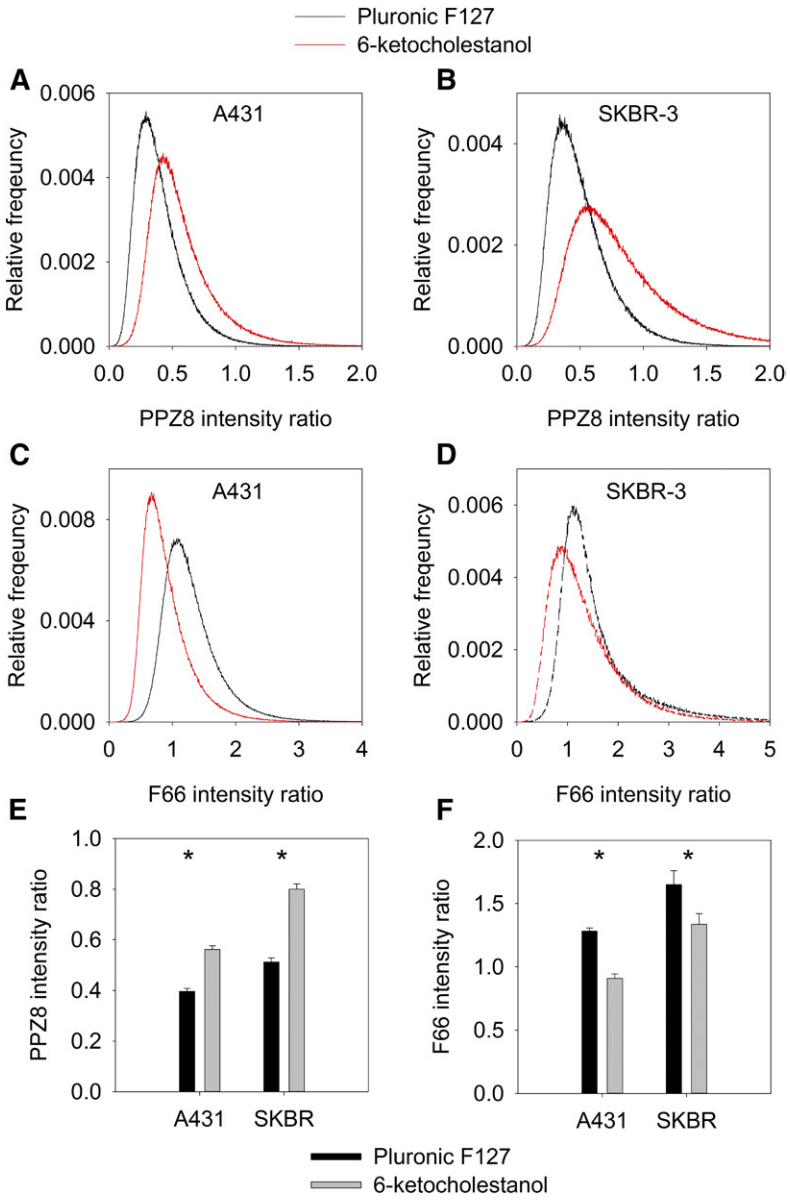

Fig. 1. The effect of an increased dipole potential on the emission ratio of PPZ8 and F66. A–D: A431 (A, C) and SKBR-3 (B, D) cells were treated with the dipole potential-increasing sterol, 6-ketocholestanol, and control cells were treated only with Pluronic F-127. Cells were labeled with the dipole potential-sensitive indicators PPZ8 or F66, followed by determining the emission ratio on a pixel-by-pixel basis. Representative histograms display the distribution of pixelwise ratios calculated from single cells. The mean intensity ratios of control (Pluronic F-127) and 6-ketocholestanol-treated cells calculated from 20 to 30 cells are displayed (E, F). The error bars represent the standard errors of the mean. *$P < 0.05$, significant difference found between the control and 6-ketocholestanol-treated cells by three-way ANOVA, followed by Tukey's honest significance test (HSD) test.

may have led to contamination of the cell membrane-derived signal with fluorescence from intracellular organelles. To rule out the contribution of internalized fluorescent dyes to the measured signal, we recorded confocal sections of the middle plain of cells, showing that the dipole potential-sensitive dyes are retained in the plasma membrane for the duration of our experiments (supplemental Fig. S3).

To get an independent confirmation of the results, we also investigated the relationship between a nonraft marker, transferrin receptor (47), and the dipole potential. The excitation ratio of di-8-ANEPPS correlated negatively with the distribution of fluorescently labeled transferrin in both SKBR-3 and A431 cells, implying that the dipole potential is weaker in nonraft domains than in rafts (Table 1, supplemental Fig. S2).

We feared that the Pearson correlation coefficient determined previously might be biased because of the presence of bright patches of the raft markers. Therefore, the correlation between the dipole potential and the raft markers was also determined by ignoring the brightest areas (supplemental Fig. S1E). The results confirmed that the dipole potential is correlated with the presence of lipid rafts even if large clusters of lipid rafts are ignored (Table 1).

The dipole potential is higher inside lipid rafts than outside them

Although the results presented in the previous section convincingly show that the dipole potential correlates positively with the localization of lipid rafts, they do not reveal how much the dipole potential differs in lipid rafts and in the bulk phase of the membrane. Cells transfected with GFP-GPI or labeled with CTX-B were stained with the dipole potential-sensitive dyes di-8-ANEPPS or F66. Images acquired from the bottom of the cells were segmented into raft and nonraft regions on the basis of their GFP-GPI or CTX-B intensities. The average di-8-ANEPPS or F66 intensity ratios were separately determined for individual pixels in the "raft" (CTX-B high and GFP-GPI high) and "nonraft"

JOURNAL OF LIPID RESEARCH ASBMB JLR

TABLE 1. Correlation between the dipole potential and lipid raft markers

	A431				SKBR-3			
	Mean ± SEM	Confidence Interval for $r = 0$		n	Mean ± SEM	Confidence Interval for $r = 0$		n
CTX-B vs. GFP-GPI	0.55 ± 0.04	−0.01	0.02	18	0.48 ± 0.03	−0.01	0.02	19
CTX-B vs. GFP-GPI (ignoring bright patches)	0.29 ± 0.04	−0.03	0.05	10	0.37 ± 0.04	−0.01	0.02	10
di-8-ANEPPS ratio vs. CTX-B	0.31 ± 0.03	−0.02	0.03	14	0.32 ± 0.02	−0.01	0.02	18
di-8-ANEPPS ratio vs. CTX-B (ignoring bright patches)	0.17 ± 0.05	−0.01	0.03	10	0.2 ± 0.04	−0.01	0.03	10
di-8-ANEPPS ratio vs. GFP-GPI	0.32 ± 0.03	−0.01	0.01	16	0.32 ± 0.03	−0.02	0.01	15
di-8-ANEPPS ratio vs. GFP-GPI (ignoring bright patches)	0.18 ± 0.05	−0.01	0.01	18	0.21 ± 0.05	−0.02	0.01	18
di-8-ANEPPS ratio vs. AC8 anti-cholesterol mAb	0.16 ± 0.02	−0.02	0.03	10	0.21 ± 0.02	−0.01	0.02	10
di-8-ANEPPS ratio vs. transferrin	−0.25 ± 0.02	−0.01	0.03	15	−0.22 ± 0.02	−0.01	0.03	15
F66 ratio vs. CTX-B	−0.54 ± 0.02	−0.004	0.02	30	−0.50 ± 0.02	−0.01	0.02	32
F66 ratio vs. CTX-B (ignoring bright patches)	−0.47 ± 0.03	−0.01	0.02	18	−0.41 ± 0.03	−0.01	0.02	18
PPZ8 vs. CTX-B	−0.55 ± 0.02	−0.01	0.01	22	−0.47 ± 0.02	−0.01	0.02	38
PPZ8 vs. CTX-B (ignoring bright patches)	−0.45 ± 0.05	−0.02	0.02	18	−0.39 ± 0.03	−0.01	0.02	18

A431 and SKBR-3 cells were labeled with the fluorescent markers displayed in the first column, followed by determining the Pearson correlation coefficient between them. The analysis was carried out in the whole cell ("cell mask" in supplemental Fig. S1) or ignoring bright patches ("cell mask ignoring bright patches" in supplemental Figure S1). The quality of the images of cells labeled with the anticholesterol antibody or with transferrin did not allow the analysis ignoring bright patches. The mean (±SEM) of the correlation coefficients determined from n number of different images as well as the 95% CI assuming no correlation ($r = 0$) are displayed in the table.

regions, and the ratio determined for the raft region was normalized to that calculated for the nonraft region in every cell (supplemental Fig. S4). Consistent with our previous results, the di-8-ANEPPS excitation ratio was significantly higher in raft regions than in nonraft regions in both A431 and SKBR-3 cells, whereas an opposite relationship was revealed between the emission ratio of F66 and the lipid raft marker CTX-B (**Fig. 2**). Given the opposite orientation of the fluorophores in the two dipole potential-sensitive dyes, both of these findings imply that the dipole potential is higher in rafts than in the rest of the membrane. The difference between the raft and nonraft regions is further demonstrated by the distributions of the intensity ratios of the dipole potential-sensitive dyes inside and outside lipid rafts. Although the di-8-ANEPPS excitation ratio shifted to larger values in "CTX-B high" and in "GFP-GPI high" regions, the emission ratio of F66 shifted to smaller values in "CTX-B high" areas when compared with "nonraft" regions (supplemental Fig. S5). These observations confirmed the hypothesis that the magnitude of the dipole potential is larger in raft microdomains than in other regions of the living cell membrane.

We also measured the emission spectra of the 3-hydroxyflavone dyes inside and outside lipid rafts to estimate the magnitude of the spectral changes. The emission spectrum was measured for each individual pixel, and they were separately averaged for pixels in the raft and nonraft regions (**Fig. 3**). The most notable difference between the two spectra was the significantly lower intensity in the nonraft regions compared with raft pixels because of water-induced quenching of fluorescence outside rafts (see the Discussion section for details). Although both the N* and T* species contribute significantly to the emission of F66 in the 460–520 and 550–600 nm regions, respectively, PPZ8 exhibits practically no peak in the spectral region corresponding to the N* species. This phenomenon can explain the inability of PPZ8 to faithfully report the dipole potential difference inside and outside lipid rafts. We determined the emission ratio of F66 inside and outside rafts by integrating the emission spectrum in the spectral range corresponding

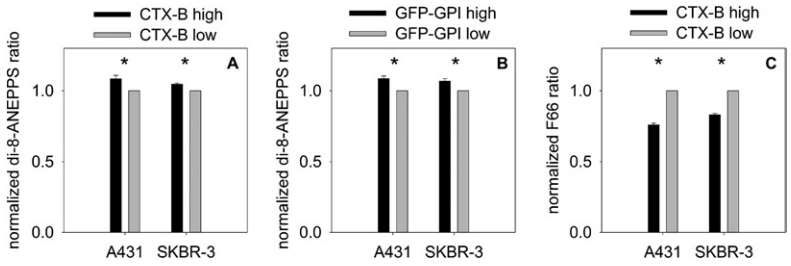

Fig. 2. Determination of the dipole potential inside and outside lipid rafts. SKBR-3 and A431 cells were transfected with GFP-GPI or labeled with AlexaFluor647-CTX-B. Labeling with the dipole potential-sensitive dyes, di-8-ANEPPS (A, B) and F66 (C), was carried out 2 days after transfection with GFP-GPI or concomitantly with CTX-B staining. Images were segmented to raft (CTX-B high, GFP-GPI high) and nonraft (CTX-B low, GFP-GPI low) regions, as is shown in supplemental Fig. S4, and the intensity ratios characteristic of the dipole potential were determined separately for the two masks. The intensity ratios were normalized to the ratio determined for the nonraft region in every cell. The error bars represent the standard errors of the mean. *$P < 0.05$, significant difference found between the intensity ratios inside and outside lipid rafts by two-way ANOVA, followed by Tukey's HSD test.

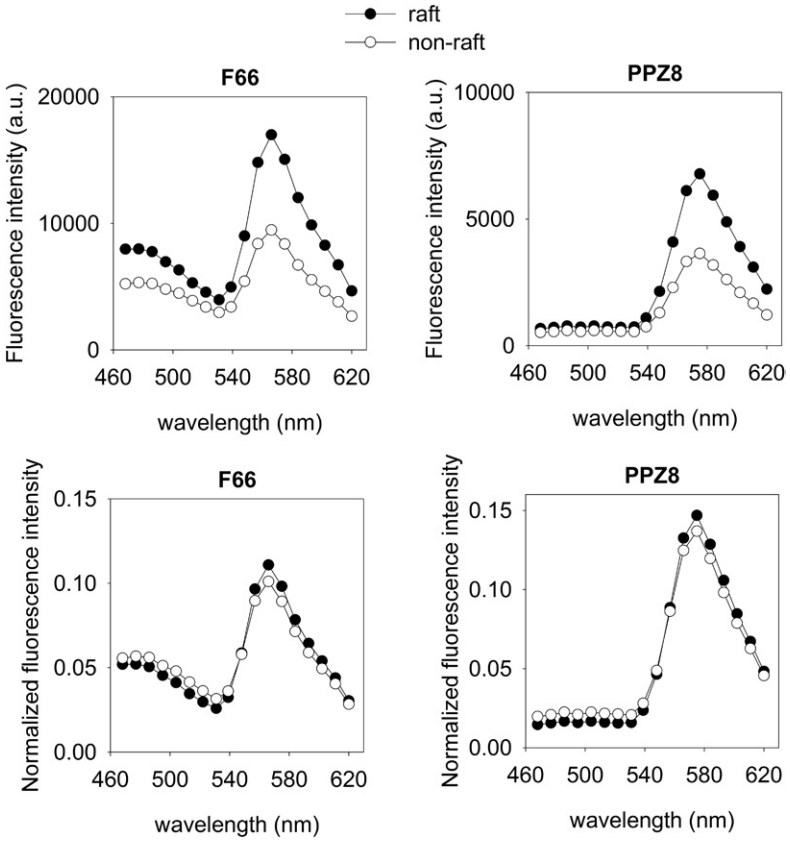

Fig. 3. Emission spectra of F66 and PPZ8 inside and outside lipid rafts. Cells were labeled with the dipole potential sensitive dyes F66 or PPZ8 and with the lipid raft marker, AlexaFluo647-CTX-B. The emission spectrum of the dipole potential-sensitive dyes was recorded on a pixel-by-pixel basis (a.u., arbitrary units). Lipid rafts correspond to high-intensity areas identified in the CTX-B images. The emission spectra were averaged separately for pixels in the raft and nonraft regions. Nonnormalized spectra are shown in the top panels. To cancel the effect of water quenching, we normalized spectra to the total fluorescence emission, and these normalized curves are shown in the bottom panels.

to the N* and T* species both in the presence and absence of 6-ketocholestanol treatment (**Table 2**). The results imply that 6-ketocholestanol changes the emission ratio of F66 approximately to the same extent inside and outside rafts, implying that it increases the dipole potential similarly in both membrane microdomains.

Sphingolipid accumulation characteristic of Gaucher's disease increases the dipole potential

Because the magnitude of the membrane dipole potential is mainly determined by the lipid composition, it can be altered in diseases in which the composition of the cell membrane changes. Because Gaucher's disease has been shown to lead to significant alterations in the lipid content of cell membranes in general and lipid rafts in particular (38, 39, 52), we tested whether these changes are substantial enough to alter the dipole potential in an in vitro model of Gaucher disease. Control and Gaucher-type, THP1-derived macrophages were labeled with di-8-ANEPPS, PPZ8, or F66, followed by acquiring confocal microscopic images in which the fluorescence intensity ratio, characteristic of the dipole potential, was evaluated in membrane pixels only. CBE treatment, inducing the Gaucher phenotype, led to a significant increase in the excitation ratio of di-8-ANEPPS and in the emission ratio of PPZ8, while causing a significant decrease in the emission ratio of F66 (**Fig. 4**). Results obtained with the three dipole potential-sensitive fluorophores strongly support that sphingolipid accumulation, characteristic of Gaucher's disease, significantly increases the magnitude of dipole potential in the cell membrane. Our findings suggest that relevant changes in the raft-like lipid composition due to pathological conditions can change the dipole potential in living cells, which might possibly play a role in the pathomechanism of these diseases.

TABLE 2. The dipole potential inside and outside lipid rafts in the presence or absence of 6-ketocholestanol treatment

	N*:T* Emission Ratio of F66	
	Raft (CTX-B high)	Nonraft (CTX-B low)
Pluronic F-127	0.54 ± 0.01	0.67 ± 0.02
6-Ketocholestanol	0.37 ± 0.02	0.46 ± 0.04

Cells were treated with 6-ketocholestanol, or control samples were incubated only with Pluronic F-127, followed by labeling with the dipole potential-sensitive dye F66 and the lipid raft marker, AlexaFluo647-CTX-B. The emission ratio of F66, characteristic of the dipole potential, was evaluated separately for the raft and nonraft regions on the basis of segmentation of the CTX-B image, and its mean (±SEM) calculated from ~10 cells is shown in the table.

DISCUSSION

Although the dipole potential generates a strong electric field in the plasma membrane, its potential biological effects are largely neglected and overlooked because of the difficulties in examining it in living cells. Because cholesterol, membrane compactness, and lipid order have been shown to affect the dipole potential, it was reasonable to assume that the dipole potential is different in liquid-ordered, raft-like membrane microdomains than in the bulk membrane (2, 5, 16). However, no such correlation has

JOURNAL OF LIPID RESEARCH ASBMB

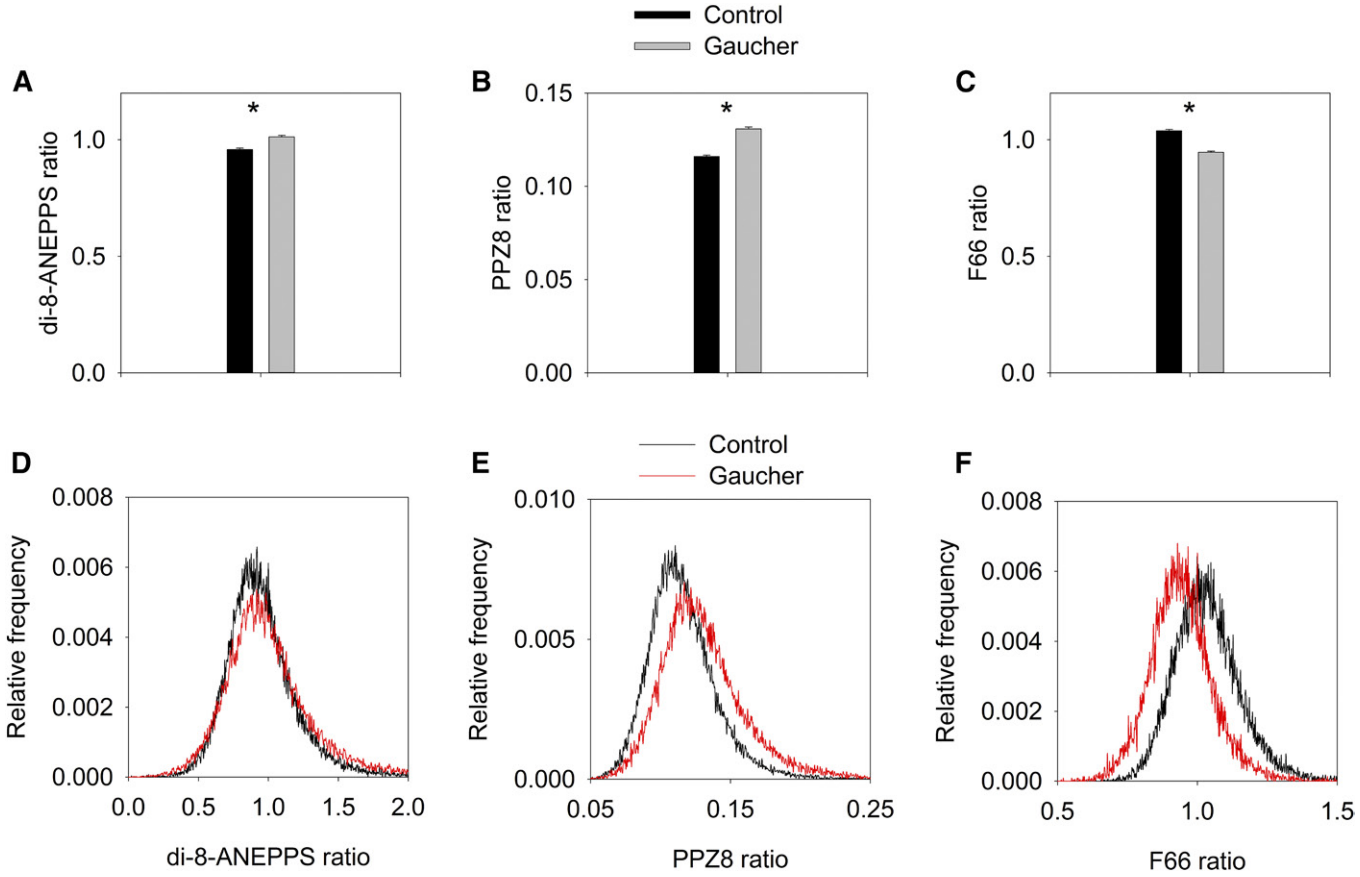

Fig. 4. Effect of sphingolipid accumulation in a model of Gaucher's disease on the dipole potential. THP-1 monocytes were differentiated to macrophages with PMA in the absence (control) and presence (Gaucher) of CBE, followed by labeling them with three different dipole potential-sensitive dyes: di-8-ANEPPS (A, D), PPZ8 (B, E), and F66 (C, F). The intensity ratios were calculated in 20–30 cells, and their means (±SEM) are displayed in the bar graphs (A–C). Representative histograms showing the distribution of pixelwise fluorescence ratios are displayed in (D–F). $*P < 0.05$, significant difference found between the intensity ratios in control and Gaucher-type cells by two-way ANOVA, followed by Tukey's HSD test.

been established in the membrane of living cells. Therefore, the major aims of this article were *a*) to present evidence for the difference in the dipole potential inside and outside lipid rafts; *b*) to estimate the magnitude of this difference; and *c*) to show how large an effect the altered lipid composition of the plasma membrane in metabolic disorders (e.g., Gaucher disease) has on the dipole potential.

Using quantitative evaluation of the Pearson correlation coefficient between lipid raft markers and the fluorescence of dipole potential-sensitive dyes, we showed that the dipole potential is positively correlated with lipid rafts (Table 1). An independent confirmation of the difference in the dipole potential inside and outside rafts was provided by labeling nonraft domains showing that the dipole potential is weaker in transferrin-labeled nonraft domains than in lipid rafts. The significance of these correlations was evaluated in two ways. The methodological or technical significance was corroborated by the fact that the correlation coefficients were always outside the 95% CI calculated for the absence of correlation. To appreciate the biological significance of the finding, we determined the correlation coefficient between two lipid raft markers. Because the correlation coefficients between the dipole potential and lipid raft markers were similar in magnitude to the positive control, that is, the correlation coefficient between the two lipid raft markers, we conclude that the observed correlation is strong and biologically meaningful.

Evaluation of the intensity ratio inside and outside lipid rafts enabled us to estimate the magnitude of the lipid raft-dependent increase in the dipole potential. Because a 15% change in the excitation ratio of di-8-ANEPPS represents a 100 mV change in the dipole potential (48), a difference of ~7% in the excitation ratio of di-8-ANEPPS measured inside and outside lipid rafts corresponds to a ~50 mV alteration in the dipole potential. An independent way of estimating the magnitude of the raft-dependent increase in the dipole potential is to compare the changes in the emission ratio of F66 induced by 6-ketocholestanol and by the presence of lipid rafts. We analyzed the dipole potential and its 6-ketocholestanol-induced alteration inside and outside lipid rafts by using a more reliable indicator, F66 (Table 2). 6-Ketocholestanol altered the emission ratio of F66 by ~35% both inside and outside lipid rafts, implying that its effect on the dipole potential is identical in both domains of the membrane. We have shown previously that 6-ketocholestanol induces ~25% increase in the excitation ratio of di-8-ANEPPS (12), corresponding to a ~160–170 mV change in the dipole potential according to the calibra-

tion of Zhang (48). Assuming that the 35% change in the emission ratio of F66, induced by 6-ketocholestanol, corresponds to a 160–170 mV difference in the dipole potential, a difference of ~20% in the emission ratio of F66 observed inside and outside lipid rafts is equivalent to a difference of ~100 mV. Given the large variation in the calculated or measured values of the dipole potential, the two estimations outlined above are in reasonable agreement with each other.

Although the relationship between lipid rafts and the dipole potential is made stronger by the presence of large, raft-like domains in the membrane, the correlation is still present if these aggregated patches are excluded from the calculations. The correlation coefficient between the dipole potential and lipid raft localization excluding large, raft-like patches is typically ~50–80% of that including aggregated lipid rafts. Although lipid rafts are assumed to be miniscule, transient, and dynamic entities (22), they are believed to aggregate upon activation (23). Therefore, the correlation between the dipole potential and lipid rafts both including and excluding large, aggregated domains is biologically relevant.

Although the correlation among three lipid raft markers, GFP-GPI, CTX-B, and the anticholesterol antibody, and two dipole potential sensitive indicators, F66 and di-8-ANEPPS, implies the existence of a stronger dipole potential in lipid rafts, the results obtained with the indicator PPZ8 are in disagreement with those collected with the other indicators (Table 1). In order to explain this contradiction, the photophysical properties of 3-hydroxyflavone dyes, F66 and PPZ8, must be taken into account (53). These dyes are present in two different ground-state forms: *1*) a hydrogen-bonded form (hydrated, H-N); and *2*) a nonhydrogen-bonded form. The latter one undergoes ESIPT to produce emission from two different molecular species, the normal form (N*) and its tautomeric variant (T*). The ratio of emission from the N* and T* species is sensitive to the dipole potential. Besides the dipole potential, other factors also affect the fluorescence of 3-hydroxyflavone dyes: *1*) the relative contribution of the H-N species depends on the hydration of the membrane, that is, the ability of water to penetrate the membrane and form hydrogen bonds with the indicator; and *2*) membrane hydration also leads to quenching of fluorescence from all three molecular species (54). In the case of F66 an increased dipole potential leads to a relative increase in the emission from species T* at the expense of species N* (supplemental Fig. S6). However, these changes are confounded by less water quenching in lipid rafts, resulting in stronger fluorescence from raft-localized indicators from all three species (Fig. 3). The lower hydration of the membrane in liquid-ordered domains has also been supported by measurements with Laurdan (55). The intensity ratio of 3-hydroxyflavone dyes is calculated as the emission in the low-wavelength range divided by that in the high-wavelength range. Both the N* and H-N species contribute to emission in the low-wavelength range. For F66 the emission ratio is expected to be negatively correlated with the dipole potential, that is, the emission in the low- and high-wavelength range should decrease and increase, respectively, in lipid rafts compared to the bulk phase. Because contributions of both the N* and H-N species decrease in lipid rafts in the low-wavelength region, the emission ratio will change as expected. The behavior of PPZ8 differs in two respects: *1*) it has hardly any emission in the low-wavelength range, leading to potential problems related to background subtraction and consequent misestimation of the specific fluorescence intensity; and *2*) the higher dipole potential and less hydration in lipid rafts are expected to change the relative contribution of the N* and H-N bands in different directions. Because the emission from the dominating T* band increases because of less water quenching in lipid rafts, the emission in the low-wavelength range of PPZ8 should increase substantially, so that its emission ratio displays the expected positive correlation with the higher dipole potential in lipid rafts. However, the intensity in the low-wavelength range of PPZ8 cannot increase strongly enough owing to points 1–2, above. Because this reasoning provided only a semiquantitative explanation for the observations, we have tried spectral unmixing according to Klymchenko (56) and singular value decomposition (57), but none of them could resolve the spectra of the individual N*, T*, and H-N species, most likely due to the limited number of data points present in the emission spectra recorded in microscopy.

The dipole potential has been shown to affect a wide range of biological phenomena because of the fact that its strong electric field modifies the conformation and clustering of membrane proteins (6–12). The magnitude of the dipole potential has been estimated to be in the range between 200 and 500 mV (3, 25). Because the estimated difference between the dipole potential inside and outside lipid rafts is 50–100 mV, this effect is expected to have a significant impact on how membrane-related phenomena, for example, transmembrane transport, signaling, and membrane trafficking, involving membrane proteins occur inside and outside lipid raft microdomains. Differences in the lipid composition and order of the membrane can influence the dipole potential and membrane-related phenomena not only under physiological conditions but also in diseases. The increase in the dipole potential associated with sphingolipid accumulation in an in vitro model of Gaucher's disease (38, 39, 52) was found to be similar in magnitude to the difference in the dipole potential inside and outside rafts (Figs. 2, 4). Because alterations in the cholesterol and sphingolipid content of the membrane in a conditional glucocerebrosidase knock-out mouse model are comparable to those observed in the in vitro model we applied, the presented results imply that pathological changes in the lipid content of the cell membrane in human diseases in general, and in Gaucher disease in particular, can lead to significant changes in the dipole potential and can also substantially modify the functioning of membrane proteins, potentially contributing to the development of disease symptoms (38, 52, 58).

In conclusion, we have shown that the dipole potential is significantly larger in lipid raft microdomains than in the bulk membrane domain. The magnitude of this difference is large enough so that the conformation of the

JOURNAL OF LIPID RESEARCH ASBMB

transmembrane domain of proteins is altered when they move into or out of lipid rafts. Consequently, some of the biological effects linked to lipid rafts can be attributed to the larger dipole potential present in this microdomain.

REFERENCES

1. O'Shea, P. 2003. Intermolecular interactions with/within cell membranes and the trinity of membrane potentials: kinetics and imaging. *Biochem. Soc. Trans.* **31:** 990–996.
2. O'Shea, P. 2005. Physical landscapes in biological membranes: physico-chemical terrains for spatio-temporal control of biomolecular interactions and behaviour. *Philos. Trans. A Math. Phys. Eng. Sci.* **363:** 575–588.
3. Brockman, H. 1994. Dipole potential of lipid membranes. *Chem. Phys. Lipids.* **73:** 57–79.
4. Wang, L. 2012. Measurements and implications of the membrane dipole potential. *Annu. Rev. Biochem.* **81:** 615–635.
5. Richens, J. L., J. S. Lane, J. P. Bramble, and P. O'Shea. 2015. The electrical interplay between proteins and lipids in membranes. *Biochim. Biophys. Acta.* **1848:** 1828–1836.
6. Andersen, O. S., and M. Fuchs. 1975. Potential energy barriers to ion transport within lipid bilayers. Studies with tetraphenylborate. *Biophys. J.* **15:** 795–830.
7. Asawakarn, T., J. Cladera, and P. O'Shea. 2001. Effects of the membrane dipole potential on the interaction of saquinavir with phospholipid membranes and plasma membrane receptors of Caco-2 cells. *J. Biol. Chem.* **276:** 38457–38463.
8. Rokitskaya, T. I., E. A. Kotova, and Y. N. Antonenko. 2002. Membrane dipole potential modulates proton conductance through gramicidin channel: movement of negative ionic defects inside the channel. *Biophys. J.* **82:** 865–873.
9. Pearlstein, R. A., C. J. Dickson, and V. Hornak. 2017. Contributions of the membrane dipole potential to the function of voltage-gated cation channels and modulation by small molecule potentiators. *Biochim. Biophys. Acta.* **1859:** 177–194.
10. Starke-Peterkovic, T., N. Turner, P. L. Else, and R. J. Clarke. 2005. Electric field strength of membrane lipids from vertebrate species: membrane lipid composition and Na+-K+-ATPase molecular activity. *Am. J. Physiol. Regul. Integr. Comp. Physiol.* **288:** R663–R670.
11. Davis, S., B. M. Davis, J. L. Richens, K. A. Vere, P. G. Petrov, C. P. Winlove, and P. O'Shea. 2015. α-Tocopherols modify the membrane dipole potential leading to modulation of ligand binding by P-glycoprotein. *J. Lipid Res.* **56:** 1543–1550.
12. Kovács, T., G. Batta, T. Hajdu, A. Szabó, T. Váradi, F. Zákány, I. Csomós, J. Szöllősi, and P. Nagy. 2016. The dipole potential modifies the clustering and ligand binding affinity of ErbB proteins and their signaling efficiency. *Sci. Rep.* **6:** 35850.
13. Starke-Peterkovic, T., and R. J. Clarke. 2009. Effect of headgroup on the dipole potential of phospholipid vesicles. *Eur. Biophys. J.* **39:** 103–110.
14. Clarke, R. J., and D. J. Kane. 1997. Optical detection of membrane dipole potential: avoidance of fluidity and dye-induced effects. *Biochim. Biophys. Acta.* **1323:** 223–239.
15. Gross, E., R. S. Bedlack, Jr., and L. M. Loew. 1994. Dual-wavelength ratiometric fluorescence measurement of the membrane dipole potential. *Biophys. J.* **67:** 208–216.
16. Haldar, S., R. K. Kanaparthi, A. Samanta, and A. Chattopadhyay. 2012. Differential effect of cholesterol and its biosynthetic precursors on membrane dipole potential. *Biophys. J.* **102:** 1561–1569.
17. Kahya, N., D. Scherfeld, K. Bacia, B. Poolman, and P. Schwille. 2003. Probing lipid mobility of raft-exhibiting model membranes by fluorescence correlation spectroscopy. *J. Biol. Chem.* **278:** 28109–28115.
18. Bacia, K., D. Scherfeld, N. Kahya, and P. Schwille. 2004. Fluorescence correlation spectroscopy relates rafts in model and native membranes. *Biophys. J.* **87:** 1034–1043.
19. Sevcsik, E., and G. J. Schutz. 2016. With or without rafts? Alternative views on cell membranes. *BioEssays.* **38:** 129–139.
20. Eggeling, C., C. Ringemann, R. Medda, G. Schwarzmann, K. Sandhoff, S. Polyakova, V. N. Belov, B. Hein, C. von Middendorff, A. Schonle, et al. 2009. Direct observation of the nanoscale dynamics of membrane lipids in a living cell. *Nature.* **457:** 1159–1162.
21. Honigmann, A., V. Mueller, H. Ta, A. Schoenle, E. Sezgin, S. W. Hell, and C. Eggeling. 2014. Scanning STED-FCS reveals spatiotemporal heterogeneity of lipid interaction in the plasma membrane of living cells. *Nat. Commun.* **5:** 5412.
22. Kraft, M. L. 2013. Plasma membrane organization and function: moving past lipid rafts. *Mol. Biol. Cell.* **24:** 2765–2768.
23. Simons, K., and D. Toomre. 2000. Lipid rafts and signal transduction. *Nat. Rev. Mol. Cell Biol.* **1:** 31–39.
24. Simons, K., and R. Ehehalt. 2002. Cholesterol, lipid rafts, and disease. *J. Clin. Invest.* **110:** 597–603.
25. Flewelling, R. F., and W. L. Hubbell. 1986. The membrane dipole potential in a total membrane potential model. Applications to hydrophobic ion interactions with membranes. *Biophys. J.* **49:** 541–552.
26. Wang, L., P. S. Bose, and F. J. Sigworth. 2006. Using cryo-EM to measure the dipole potential of a lipid membrane. *Proc. Natl. Acad. Sci. USA.* **103:** 18528–18533.
27. Harder, E., A. D. Mackerell, Jr., and B. Roux. 2009. Many-body polarization effects and the membrane dipole potential. *J. Am. Chem. Soc.* **131:** 2760–2761.
28. Ding, W., M. Palaiokostas, W. Wang, and M. Orsi. 2015. Effects of lipid composition on bilayer membranes quantified by all-atom molecular dynamics. *J. Phys. Chem. B.* **119:** 15263–15274.
29. Yang, Y., K. M. Mayer, N. S. Wickremasinghe, and J. H. Hafner. 2008. Probing the lipid membrane dipole potential by atomic force microscopy. *Biophys. J.* **95:** 5193–5199.
30. Shrestha, R., C. M. Anderson, A. E. Cardenas, R. Elber, and L. J. Webb. 2017. Direct measurement of the effect of cholesterol and 6-ketocholestanol on the membrane dipole electric field using vibrational stark effect spectroscopy coupled with molecular dynamics simulations. *J. Phys. Chem. B.* **121:** 3424–3436.
31. Shynkar, V. V., A. S. Klymchenko, G. Duportail, A. P. Demchenko, and Y. Mely. 2005. Two-color fluorescent probes for imaging the dipole potential of cell plasma membranes. *Biochim. Biophys. Acta.* **1712:** 128–136.
32. Klymchenko, A. S., G. Duportail, Y. Mely, and A. P. Demchenko. 2003. Ultrasensitive two-color fluorescence probes for dipole potential in phospholipid membranes. *Proc. Natl. Acad. Sci. USA.* **100:** 11219–11224.
33. M'Baye, G., V. V. Shynkar, A. S. Klymchenko, Y. Mely, and G. Duportail. 2006. Membrane dipole potential as measured by ratiometric 3-hydroxyflavone fluorescence probes: accounting for hydration effects. *J. Fluoresc.* **16:** 35–42.
34. Butters, T. D. 2007. Gaucher disease. *Curr. Opin. Chem. Biol.* **11:** 412–418.
35. Sidransky, E. 2012. Gaucher disease: insights from a rare Mendelian disorder. *Discov. Med.* **14:** 273–281.
36. Simons, K., and J. Gruenberg. 2000. Jamming the endosomal system: lipid rafts and lysosomal storage diseases. *Trends Cell Biol.* **10:** 459–462.
37. Westbroek, W., A. M. Gustafson, and E. Sidransky. 2011. Exploring the link between glucocerebrosidase mutations and parkinsonism. *Trends Mol. Med.* **17:** 485–493.
38. Hein, L. K., S. Duplock, J. J. Hopwood, and M. Fuller. 2008. Lipid composition of microdomains is altered in a cell model of Gaucher disease. *J. Lipid Res.* **49:** 1725–1734.
39. Hein, L. K., P. J. Meikle, J. J. Hopwood, and M. Fuller. 2007. Secondary sphingolipid accumulation in a macrophage model of Gaucher disease. *Mol. Genet. Metab.* **92:** 336–345.
40. Ritchie, K., R. Iino, T. Fujiwara, K. Murase, and A. Kusumi. 2003. The fence and picket structure of the plasma membrane of live cells as revealed by single molecule techniques (review). *Mol. Membr. Biol.* **20:** 13–18.
41. Varma, R., and S. Mayor. 1998. GPI-anchored proteins are organized in submicron domains at the cell surface. *Nature.* **394:** 798–801.
42. Harder, T., P. Scheiffele, P. Verkade, and K. Simons. 1998. Lipid domain structure of the plasma membrane revealed by patching of membrane components. *J. Cell Biol.* **141:** 929–942.
43. Hammond, A. T., F. A. Heberle, T. Baumgart, D. Holowka, B. Baird, and G. W. Feigenson. 2005. Crosslinking a lipid raft component triggers liquid ordered-liquid disordered phase separation in model plasma membranes. *Proc. Natl. Acad. Sci. USA.* **102:** 6320–6325.
44. Raghunathan, K., T. H. Wong, D. J. Chinnapen, W. I. Lencer, M. G. Jobling, and A. K. Kenworthy. 2016. Glycolipid crosslinking is required for cholera toxin to partition into and stabilize ordered domains. *Biophys. J.* **111:** 2547–2550.

45. Duggan, J., G. Jamal, M. Tilley, B. Davis, G. McKenzie, K. Vere, M. G. Somekh, P. O'Shea, and H. Harris. 2008. Functional imaging of microdomains in cell membranes. *Eur. Biophys. J.* **37:** 1279–1289.
46. Bíró, A., L. Cervenak, A. Balogh, A. Lőrincz, K. Uray, A. Horváth, L. Romics, J. Matkó, G. Füst, and G. László. 2007. Novel anti-cholesterol monoclonal immunoglobulin G antibodies as probes and potential modulators of membrane raft-dependent immune functions. *J. Lipid Res.* **48:** 19–29.
47. Pike, L. J., X. Han, and R. W. Gross. 2005. Epidermal growth factor receptors are localized to lipid rafts that contain a balance of inner and outer leaflet lipids: a shotgun lipidomics study. *J. Biol. Chem.* **280:** 26796–26804.
48. Zhang, J., R. M. Davidson, M. D. Wei, and L. M. Loew. 1998. Membrane electric properties by combined patch clamp and fluorescence ratio imaging in single neurons. *Biophys. J.* **74:** 48–53.
49. Zeinab, D., A. K. Oleksandr, K. Rémy, R. Ludovic, V. Romain, M. Yves, and S. K. Andrey. 2013. Rational design of fluorescent membrane probes for apoptosis based on 3-hydroxyflavone. *Methods Appl. Fluoresc.* **1:** 025002.
50. Costes, S. V., D. Daelemans, E. H. Cho, Z. Dobbin, G. Pavlakis, and S. Lockett. 2004. Automatic and quantitative measurement of protein-protein colocalization in live cells. *Biophys. J.* **86:** 3993–4003.
51. Gonzalez, R. C., R. E. Woods, and S. L. Eddins. 2004. Segmentation using the watershed algorithm. *In* Digital Image Processing Using MATLAB. R. C. Gonzalez, R. E. Woods, and S. L. Eddins, editors. Pearson Prentice Hall, Upper Saddle River. 417–425.
52. Hattersley, K. J., L. K. Hein, and M. Fuller. 2013. Lipid composition of membrane rafts, isolated with and without detergent, from the spleen of a mouse model of Gaucher disease. *Biochem. Biophys. Res. Commun.* **442:** 62–67.
53. Demchenko, A. P., Y. Mely, G. Duportail, and A. S. Klymchenko. 2009. Monitoring biophysical properties of lipid membranes by environment-sensitive fluorescent probes. *Biophys. J.* **96:** 3461–3470.
54. Dobretsov, G. E., T. I. Syrejschikova, and N. V. Smolina. 2014. On mechanisms of fluorescence quenching by water. [Article in Russian] *Biofizika.* **59:** 231–237.
55. Gaus, K., T. Zech, and T. Harder. 2006. Visualizing membrane microdomains by Laurdan 2-photon microscopy. *Mol. Membr. Biol.* **23:** 41–48.
56. Klymchenko, A. S., G. Duportail, A. P. Demchenko, and Y. Mely. 2004. Bimodal distribution and fluorescence response of environment-sensitive probes in lipid bilayers. *Biophys. J.* **86:** 2929–2941.
57. Tsurui, H., H. Nishimura, S. Hattori, S. Hirose, K. Okumura, and T. Shirai. 2000. Seven-color fluorescence imaging of tissue samples based on Fourier spectroscopy and singular value decomposition. *J. Histochem. Cytochem.* **48:** 653–662.
58. Sinclair, G. B., G. Jevon, K. E. Colobong, D. R. Randall, F. Y. Choy, and L. A. Clarke. 2007. Generation of a conditional knockout of murine glucocerebrosidase: utility for the study of Gaucher disease. *Mol. Genet. Metab.* **90:** 148–156.

Supplementary Material

The dipole potential correlates with lipid raft markers in the plasma membrane of living cells

Tamás Kovács, Gyula Batta, Florina Zákány, János Szöllősi, Peter Nagy

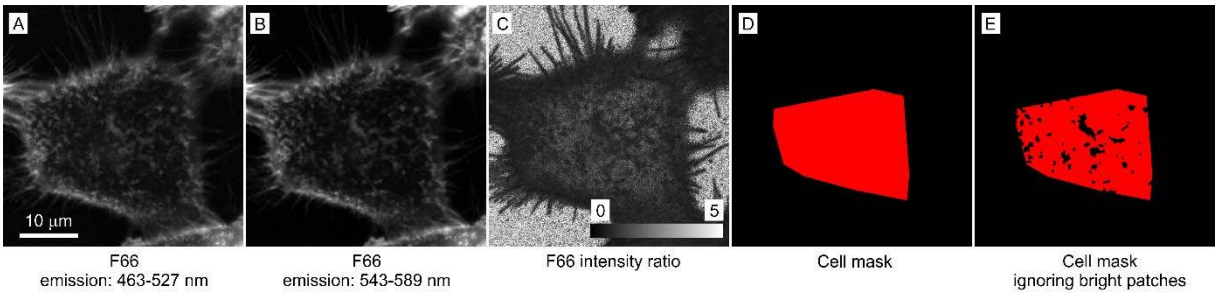

Supplemental Figure S1. Representative images showing staining of cells with the dipole potential-sensitive indicator, F66. A431 cells were treated with Pluronic F-127 followed by staining with F66. The dye was excited at 405 nm, and its emission was measured in two wavelength ranges, 463-527 nm ("blue channel", A) and 543-589 nm ("green channel", B). An emission ratio image was calculated by dividing the intensity recoded in the blue channel by the intensity in the green channel on a pixel-by-pixel basis (C). The ratio values were only evaluated in a mask, drawn manually, corresponding to the flat membrane adjacent to the coverslip (D) or within this cell mask ignoring the brightest patches (E).

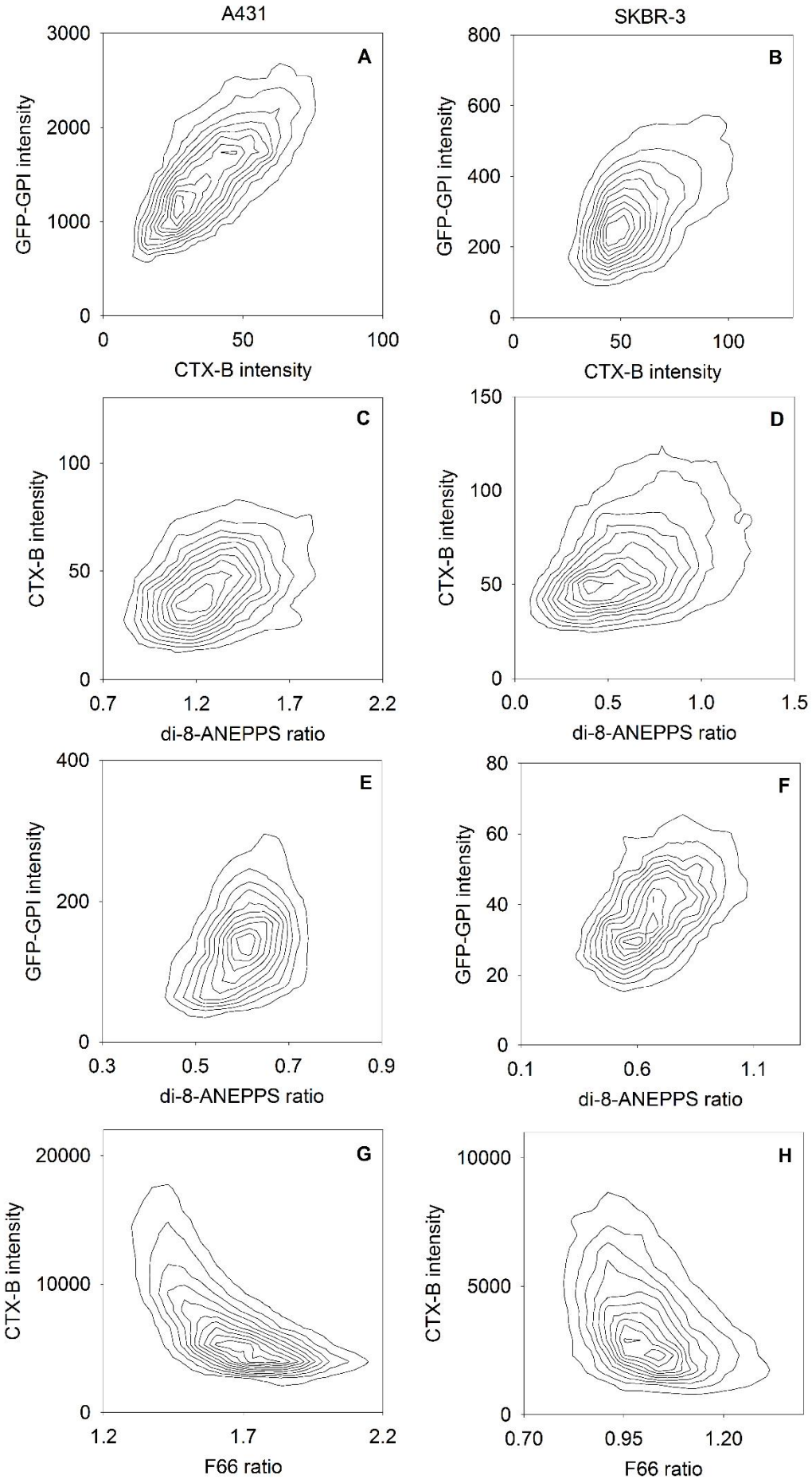
A431
SKBR-3
A
B
C
D
E
F
G
H
GFP-GPI intensity
CTX-B intensity
di-8-ANEPPS ratio
F66 ratio
3000
2000
1000
0
50
100
800
600
400
200
150
0.0
0.5
1.0
1.5
0.7
1.2
1.7
2.2
0.3
0.9
80
60
40
20
0.1
0.6
1.1
20000
10000
5000
0.70
0.95
1.20

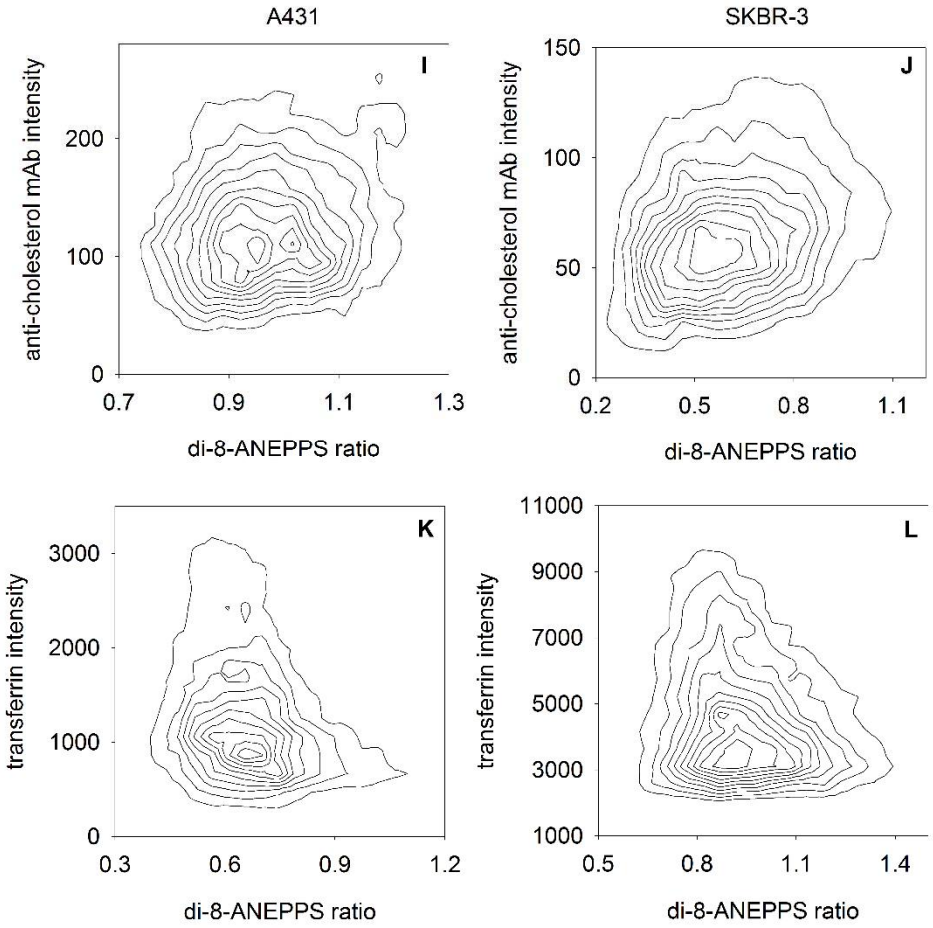

Supplemental Figure S2. Representative contour plots showing the correlation between the dipole potential and lipid raft markers. **A-B.** A431 (A) and SKBR-3 (B) cells were transfected with GFP-GPI followed by labeling them with AlexaFluor647-CTX-B two days after transfection. The correlation of the intensity of the two lipid raft markers are displayed. **C-L.** A431 (C, E, G, I, K) and SKBR-3 (D, F, H, J, L) cells were labeled with di-8-ANEPPS (C-F, I-L) or F66 (G, H) to measure their dipole potential. Transfection with GFP-GPI (E, F), labeling with AlexaFluor647-CTX-B (C, D, G, H) or with anti-cholesterol mAb (I, J) was used as a lipid raft marker. Alternatively, non-raft membrane domains were labeled with AlexaFluor647-transferrin (K, L). The correlation between the fluorescence intensity ratio of the dipole potential sensitive indicator and the membrane microdomain marker is displayed in the figures. Quantitative evaluation of these dot plots is presented in Table 1.

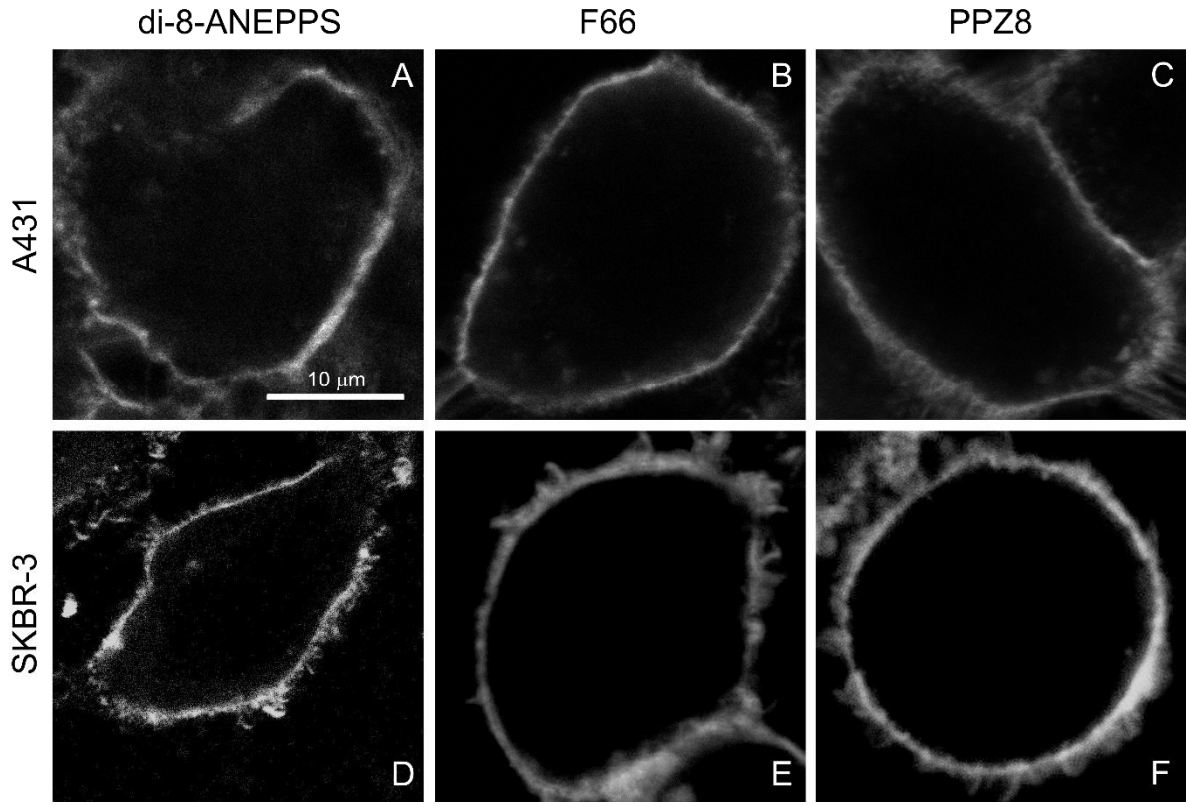

Supplemental Figure S3. Membrane localization of dipole potential-sensitive dyes. A431 (A-C) and SKBR-3 (D-F) cells were stained with di-8-ANEPPS (A, D), F66 (B, E) or PPZ8 (C, F) followed by recording confocal sections in the middle plain of cells.

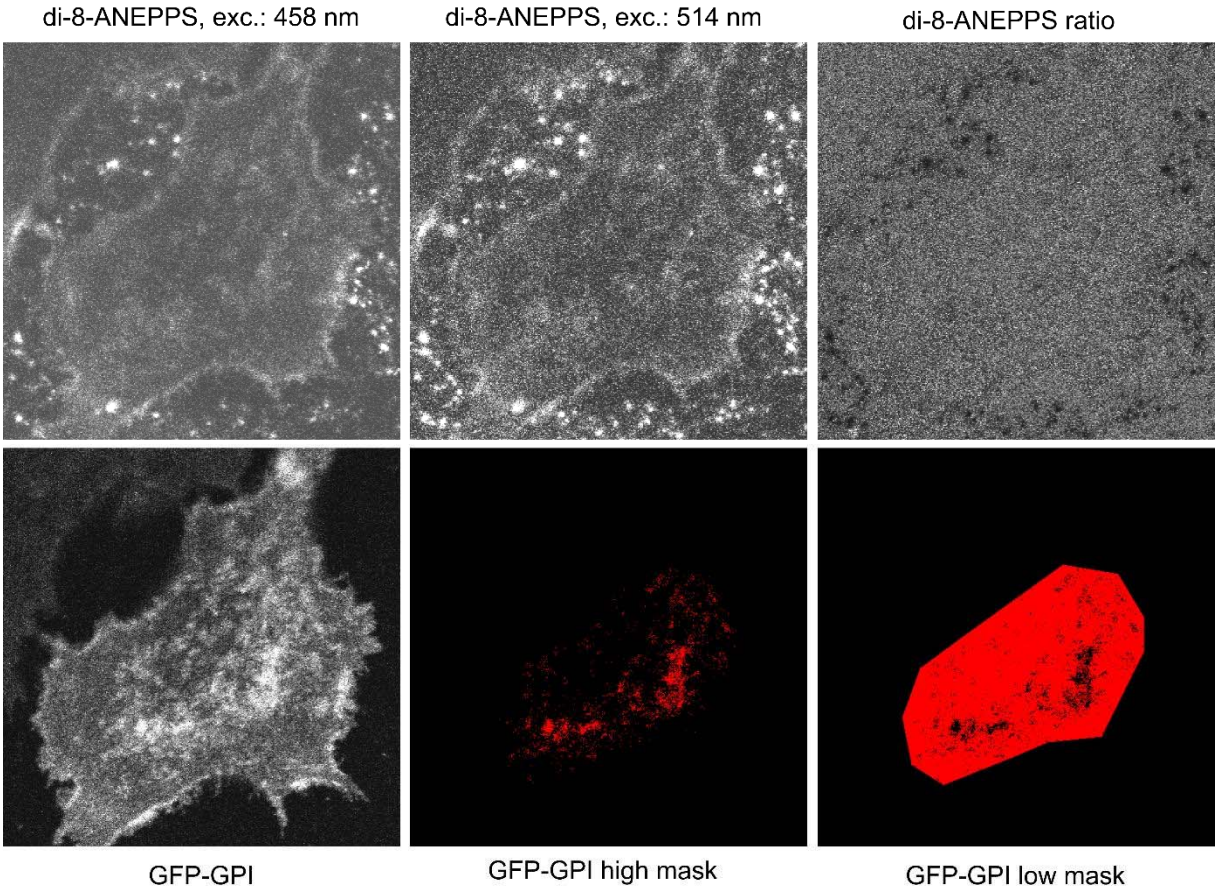

Supplemental Figure S4. Representative images showing the analysis of dipole potential inside and outside lipid rafts. SKBR-3 cells were transfected with GFP-GPI followed by staining them with di-8-ANEPPS two days after transfection. ANEPPS was excited at two different wavelengths (458 nm and 514 nm) and its emission was measured between 584 and 686 nm. The intensity recorded with an excitation of 458 nm was divided by that excited at 514 nm (di-8-ANEPPS ratio). The fluorescence of GFP-GPI was recorded in a third image which was segmented using the maxentropy algorithm. The intersection of the high intensity clusters identified by the segmentation and the cell mask drawn manually was considered to be the raft mask (GFP-GPI high mask). The intersection of the low intensity areas in the GPI-GPI image with the cell mask corresponds to the non-raft mask (GFP-GPI low mask). The di-8-ANEPPS ratio was evaluated in both masks separately.

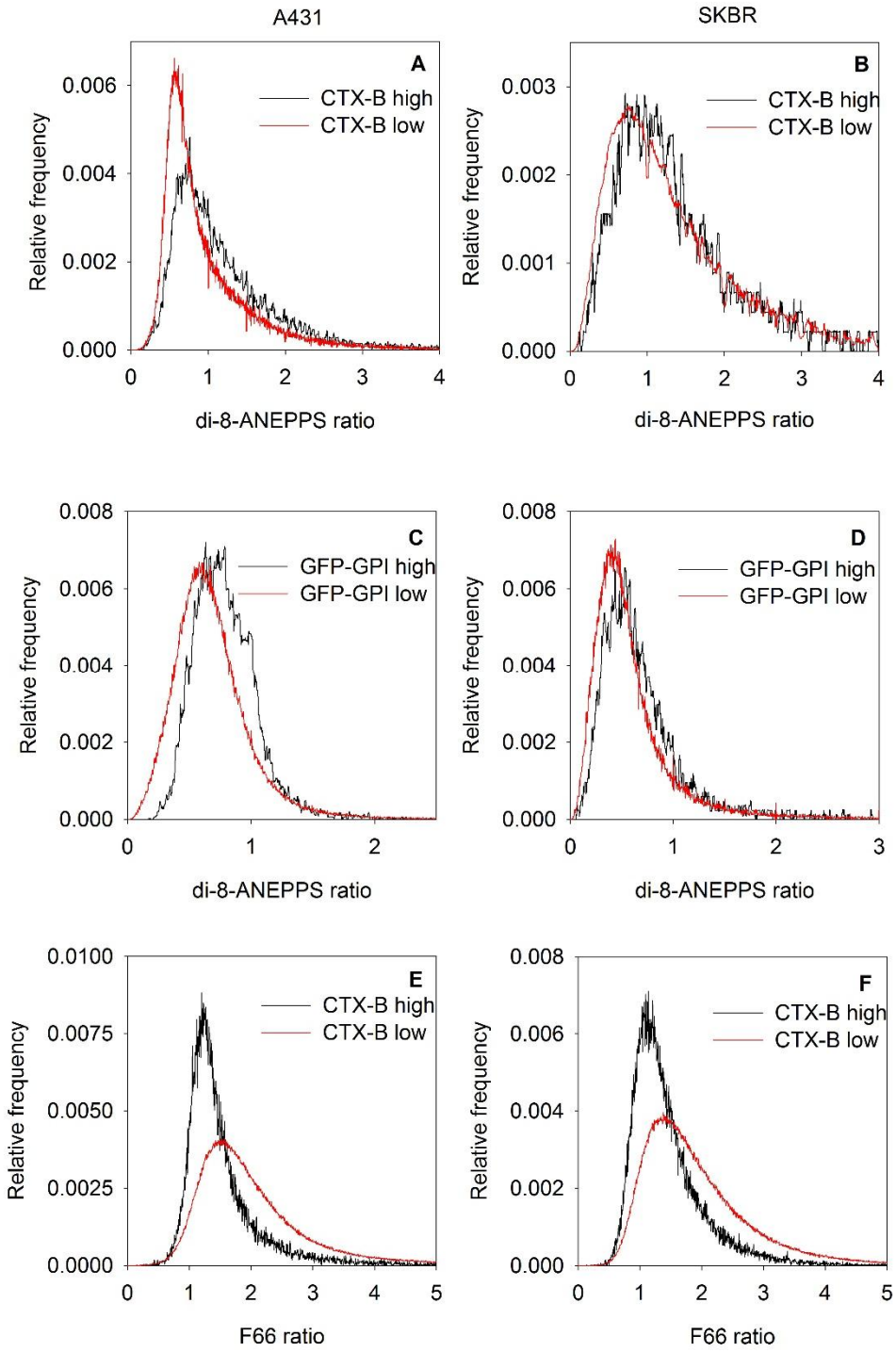

Supplemental Figure S5. The dipole potential inside and outside lipid rafts. A431 (A, C, E) and SKBR-3 (B, D, F) cells were labeled with the dipole potential sensitive dyes di-8-ANEPPS (A-D) or F66 (E, F). Lipid rafts were labeled with CTX-B staining (A, B, E, F) or GFP-GPI transfection (C, D). Images of the raft markers were segmented to produce raft and non-raft masks corresponding to high and low intensities of the raft markers, respectively, as shown in Fig. S3. The distribution of the di-8-ANEPPS excitation ratio and the F66 emission ratio was separately analyzed inside and outside lipid rafts, and their distributions are shown in the figures.

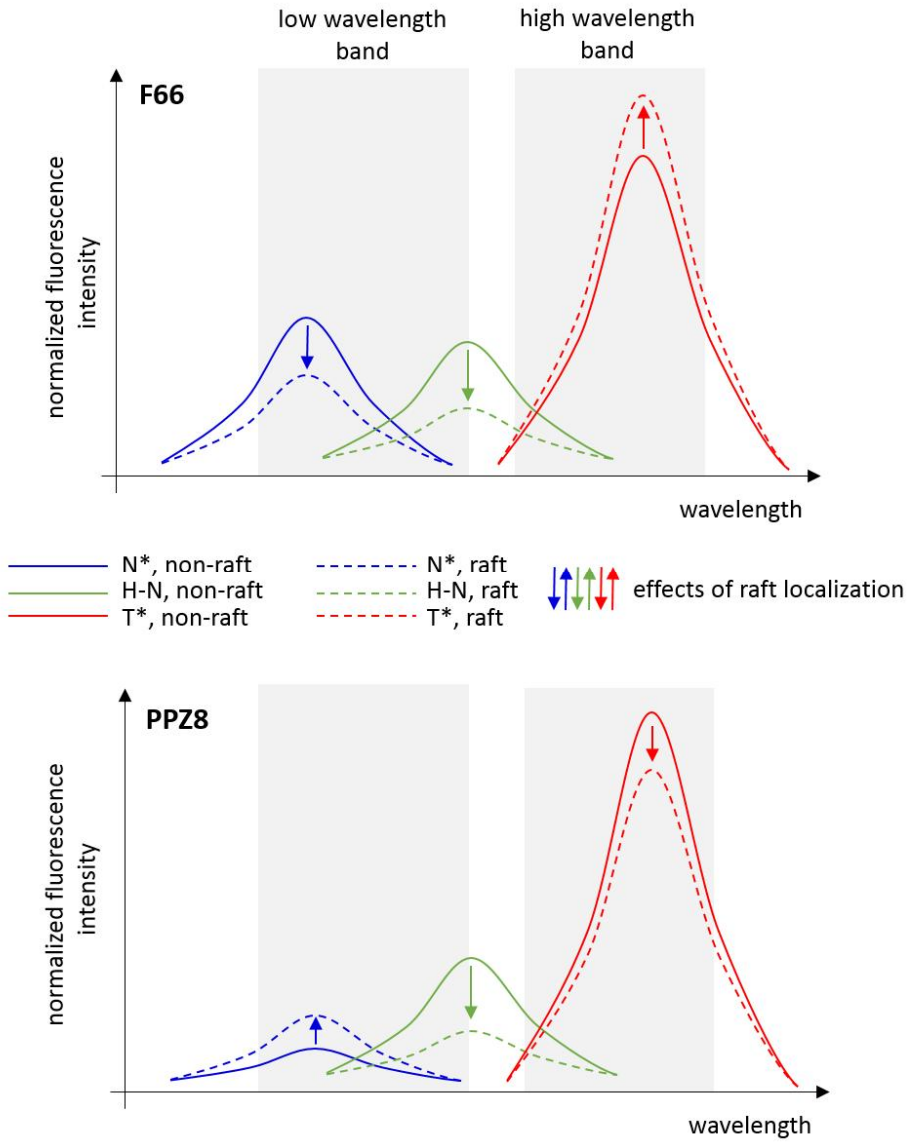

Supplemental Figure S6. Changes in the emission characteristics of 3-hydroxyflavone dyes in lipid rafts. The emission of 3-hydroxyflavone dyes originates from three different species. Species N* and T* interconvert by excited-state intramolecular proton transfer (ESIPT) and their ratio is sensitive to the dipole potential. The third species, H-N, is a hydrogen-bonded form of the dye. In the case of F66, the relative fraction of the N* species decreases upon increasing the dipole potential, while the opposite change occurs for PPZ8 due to the inverted orientation of the fluorophore. Lipid rafts not only exhibit a higher dipole potential, but also a more compact lipid structure resulting in less hydration of the membrane and a consequent decrease in the relative contribution of the H-N species to the emission and overall quenching of fluorescence from all three species. The effect of water quenching is not shown in the figure since the spectra are normalized to the total emission from the dye. Both the N* and H-N species contribute to the emission in the low wavelength range. Assuming the dipole potential is higher in lipid rafts than in the rest of the membrane the relative changes in the emission from the N* and H-N species change in the same direction for F66, but in the opposite direction for PPZ8. Therefore, the emission ratio of PPZ8, i.e. the fluorescence intensity in the low wavelength range vs. the high wavelength range, will not faithfully report the dipole potential difference between lipid rafts and non-raft regions.